Electronic Supplementary Material (ESI) for Physical Chemistry Chemical Physics.

Supplementary Information

Factors Affecting the Polarity and Magnitude of Photoresponse of Transient Photodetectors

Louisa Reissig[1‡], Kotaro Mori[1‡], Ryan Treadwell[1,2], Simon Dalgleish[1,3]*, Kunio Awaga[1,4]*

[1] Department of Chemistry and Research Centre for Material Science, Nagoya University, Furo-cho, Chikusa, 464-8602 Nagoya, Japan

[2] School of Chemistry, University of Edinburgh, West Mains Road, Edinburgh, EH9 3JJ, UK

[3] Institute for Advanced Research, Nagoya University, Furo-cho, Chikusa, 464-8601 Nagoya, Japan

[4] CREST, JST, Nagoya University, Furo-cho, Chikusa, 464-8602 Nagoya, Japan

S1: Device specifications and photocurrent measurement setup:

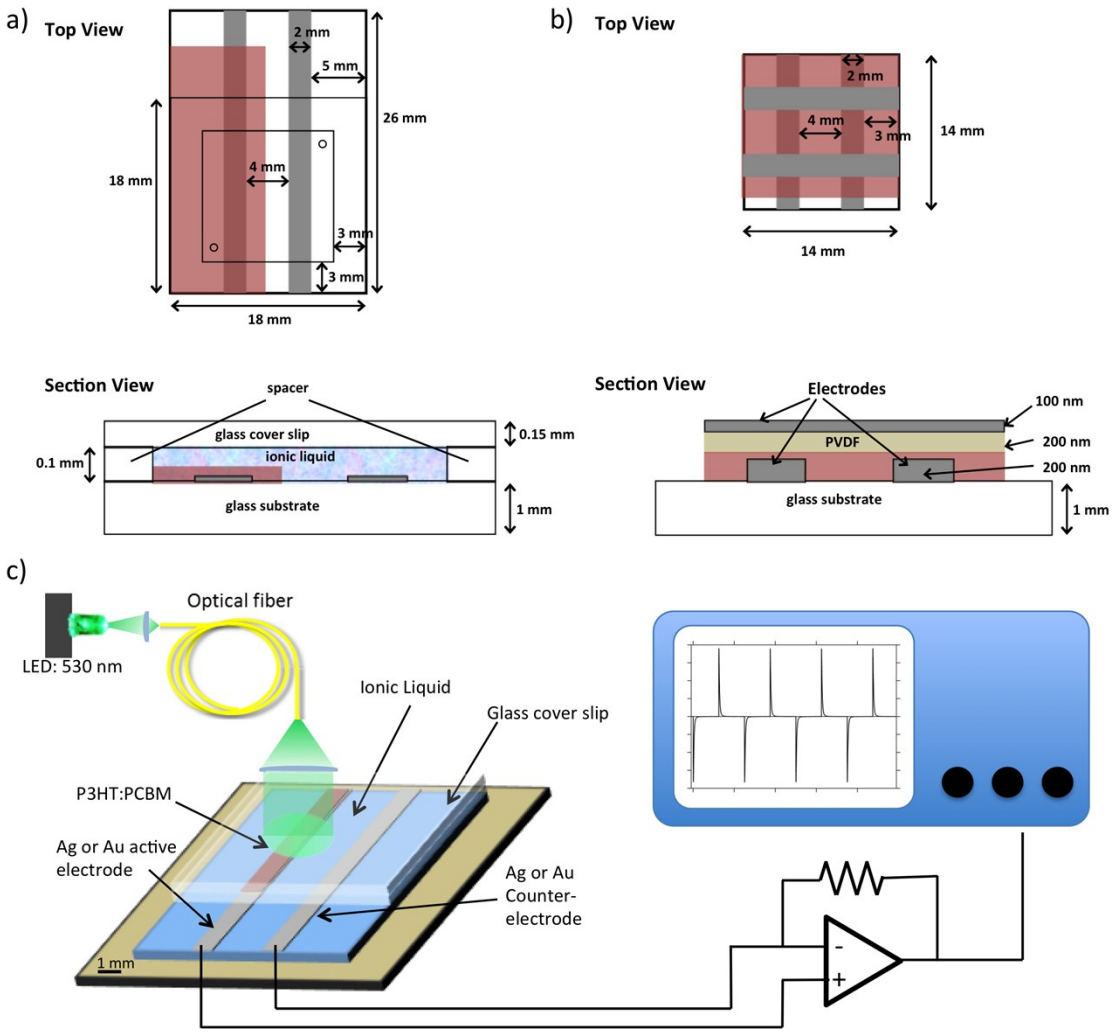

FIGURE S1: Plan and profile view, including dimensions, of a completed IL-MISM (a) and solid-state MISM (b) device used in this study. Sketch of measuring platform for photocurrent measurements (c).

Substrate fabrication: Devices were prepared on glass slides of dimensions 26 x 18 x 1 mm (or 14 x 14 x 1 mm for solid-state), pre-cleaned by mild bath ultrasonnication (45 W, isopropanol, acetone, chloroform, 10 mins. each). The slides were mounted on a shadow mask, defining electrodes of 2 x 26 mm with 4 mm separation, and inserted into a physical vapor deposition (PVD) apparatus (ULVAC). The chamber was evacuated to an initial vacuum of $4x10^{-4}$ Pa prior to deposition. Silver (Ag, 200 nm) and/or gold (Au, 200 nm + >5 nm chromium adhesion layer) were deposited at rates of 0.4 $Å s^{-1}$ (measured by quartz crystal microbalance (QCM)), masking one electrode with Kapton tape when necessary. The substrates were immediately transferred into a desiccator, where they were stored until active layer deposition.

IL-device assembly: After active layer deposition, the IL-MISM devices were completed with a glass cover slip before testing (see Fig. S1a), fixed with a thermally sealed 60 μm Surlyn spacer (Solaronix). The void was filled with ionic liquid by

capillary force through pre-drilled holes in the cover slip 6 min after removal from the desiccator, and illuminated 3 min later.

Photocurrent measurement setup (see Fig. S1c): The light was directed onto a collimator, resulting in a 7 mm homogeneous broad beam, modulated as a square-wave light signal by a function generator (Tektronix AFG320). The light power was adjusted before each experiment by a home-built driver unit (circuit diagram available upon request), and monitored by a silicon photodiode (SiPD) (FID08T13TX), calibrated by an optical power meter (ADCMT 8230E). Unless otherwise stated, a light power $P_{\text{incident}} \approx 0.88$ mWcm^{-2} was used. As the electrode size was 2 mm wide, giving an active area of ≈ 0.14 cm^2, and only 35% of the incident light contributed to the electrical response. For convention, the electrode in contact with the active layer (active electrode) was grounded. The devices were connected to an inverting transimpedance amplifier (Keithley 428), in which the transient short circuit current signal was amplified and converted into a voltage signal, which was visualized by an oscilloscope (Tektronix TDS5104B). For convention, all data was not inverted, *i.e.* a positive peak corresponds to holes being extracted from the active layer, and the first peak in a photocurrent plot corresponds to light ON. Each device was tested for a period of at least 30 min to study the effect of time on the waveform.

S2: Structure and properties of ionic liquids used in this study:

1)

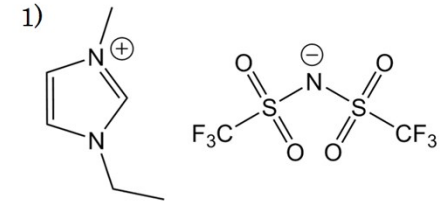

EMIM **TFSI**

1-Ethyl-3-methylimidazolium
bis(trifluoromethanesulfonyl)imidel)imide

2)

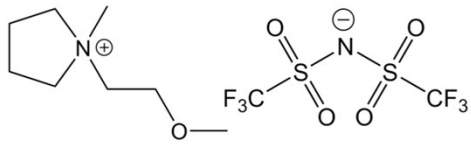

MEMP **TFSI**

N-(2-Methoxyethyl)-N-methylpyrrolidinium
bis(trifluoromethanesulfonyl)imide

3)

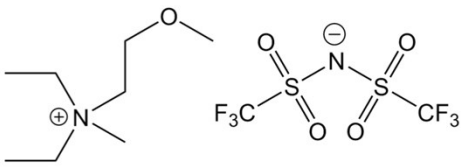

DEME **TFSI**

N,N-Diethyl-N-methyl-N-(2-methoxyethyl)ammonium
bis(trifluoromethanesulfonyl)imide

4)

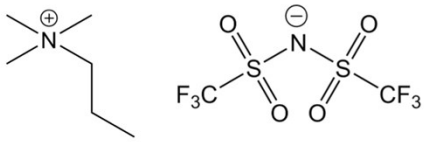

TMPA **TFSI**

Trimethylpropylammonium
bis(trifluoromethanesulfonyl)imide

5)

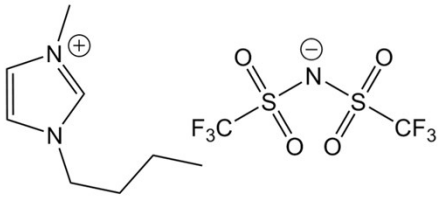

BMIM **TFSI**

1-Butyl-3methylimidazolium
bis(trifluoromethanesulfonyl)imide

6)

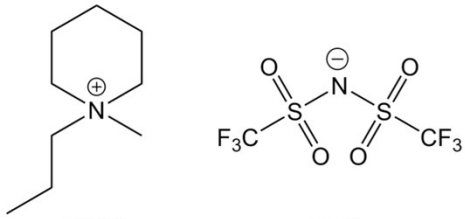

PP13 **TFSI**

N-Methyl-N-propylpiperidinium
bis(trifluoromethanesulfonyl)imide

7)

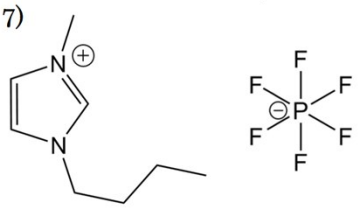

BMIM **PF_6**

1-Butyl-3-methylimidazolium
hexafluorophosphate

8)

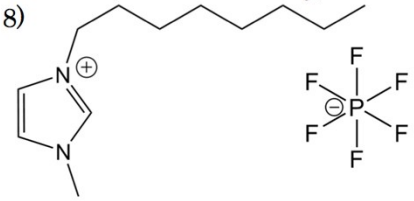

OMIM **PF_6**

1-Octyl-3-methylimidazolium
hexafluorophosphate

9)

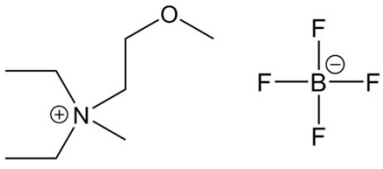

DEME **BF_4**

N,N-Diethyl-N-methyl-N-(2-methoxyethyl)ammonium
tetrafluoroborate

10)

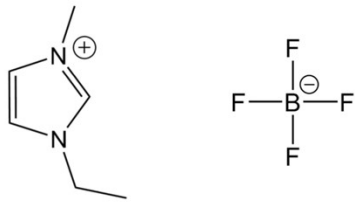

EMIM **BF_4**

1-Ethyl-3-methylimidazolium
tetrafluoroborate

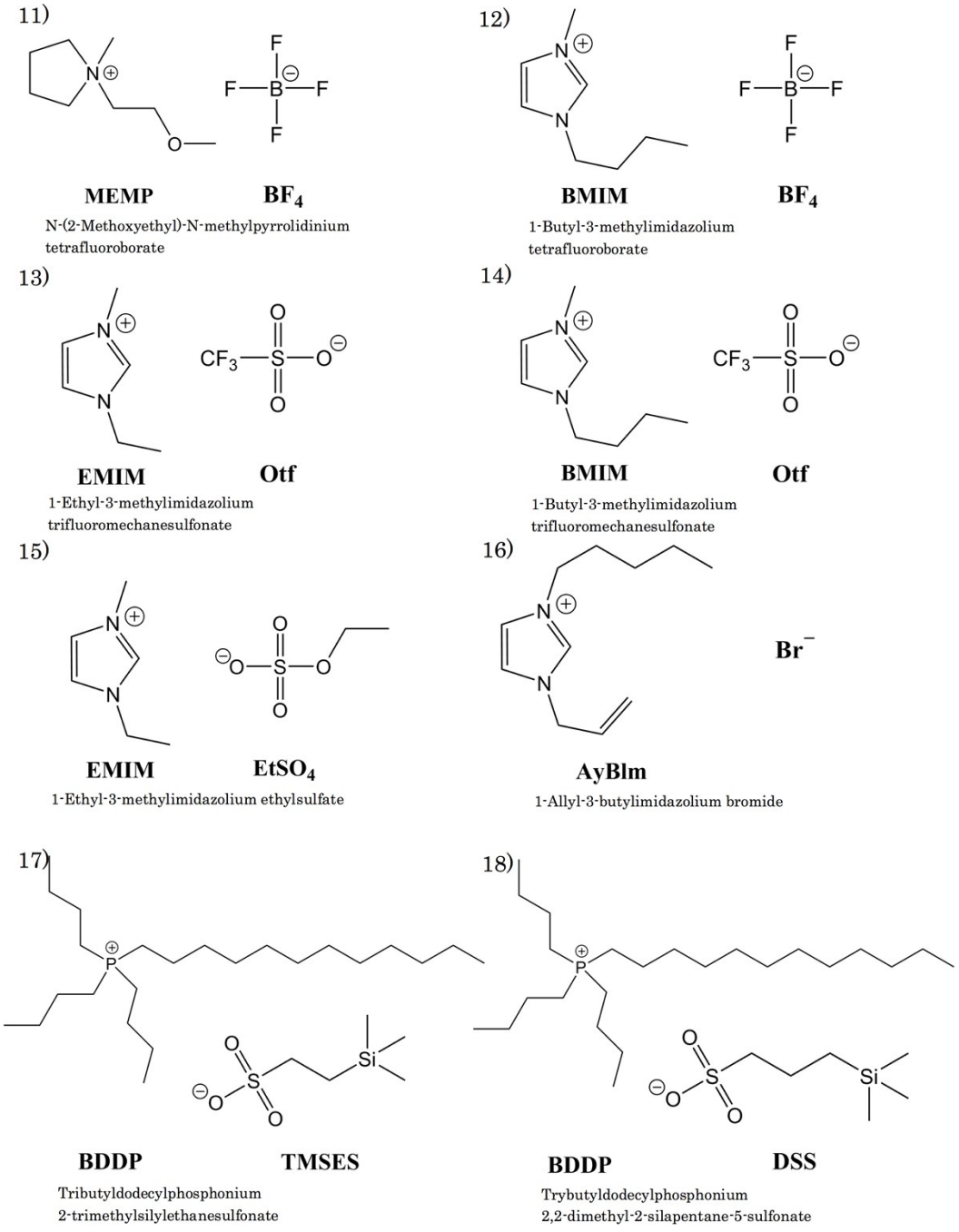

FIGURE S2: Molecular structure of the ionic liquids used in this study.

Ionic Liquid	Viscosity [cP]	Capacitance [µF/cm^2][4]
EMIM TFSI	28[1]	1.77
MEMP TFSI	50[2]	
DEME TFSI	120[3]	1.6
TMPA TFSI	72[3]	
BMIM TFSI	64[3]	2.26
PP13 TFSI	117[2]	
BMIM PF_6	272[2]	1.71
DEME BF_4	1200[3]	
EMIM BF_4	32[2]	
MEMP BF_4	154[2]	
BMIM BF_4	132[3]	1.5
BMIM Otf	92[3]	
EMIM $EtSO_4$	122[2]	
AyBlm Br	2558[2]	
BDDP TMSES	2570[2]	
BDDP DSS	2429[2]	

TABLE S2: Viscosity and capacitance values of selected ionic liquids at room temperature. The ionic liquids used for Fig. 5 are underlined.

S3: Light intensity dependence of photocurrent signal:

It should be noted that the incident light intensity had a strong effect on the signal shape (Fig. S3a). While the signal intensity I_{peak} showed a reasonably linear dependence on light intensity, giving a near constant responsivity, the extracted charge Q shows a sub-linear behavior with increasing light intensity (Fig. S3b), as reported previously.[5] The signal becomes stronger and faster with increasing light intensity, and thus all the fitting parameters strongly depend on the light intensity used, and this in a non-linear fashion. This hampers a direct comparison between devices. In the case of I_{peak}, the non-linearity is, in most cases, negligible, and thus a comparison is possible, as long as the light intensity is kept relatively constant.

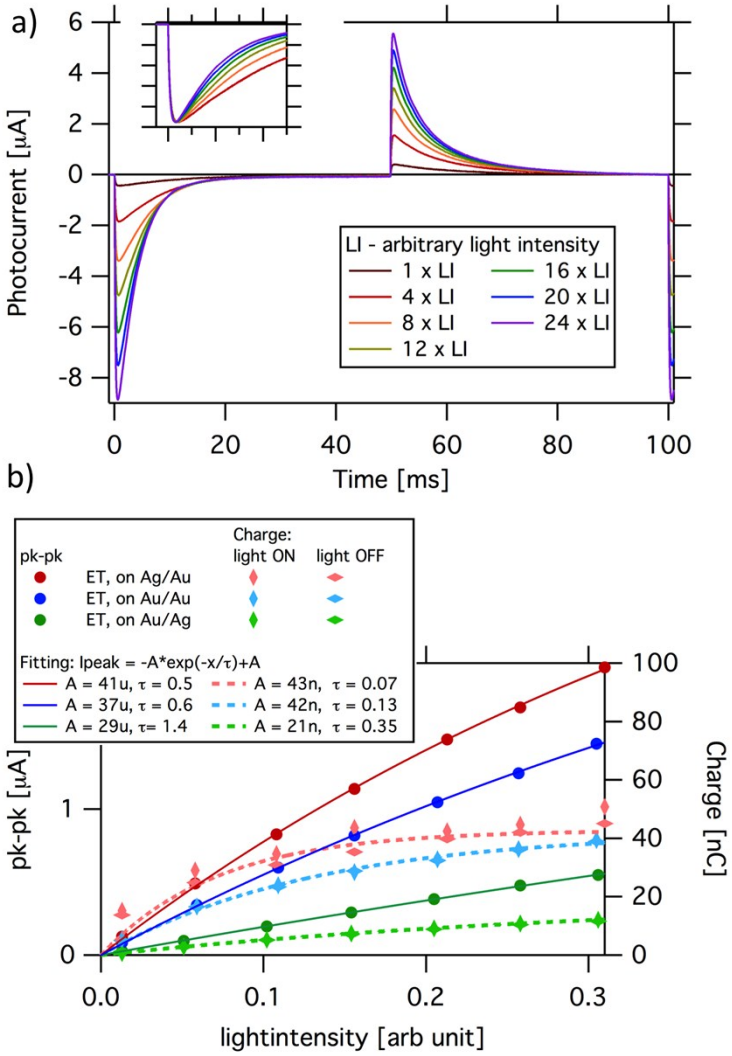

FIGURE S3a,b: Dependence of signal shape on light intensity for 1:1 blend in a Au/Au device using ET as ionic liquid (a); extracted I_{peak} *and* Q *for a 1:1 blend in Ag/Au, Au/Au, Au/Ag devices using ET as ionic liquid for a range of light intensities (b).*

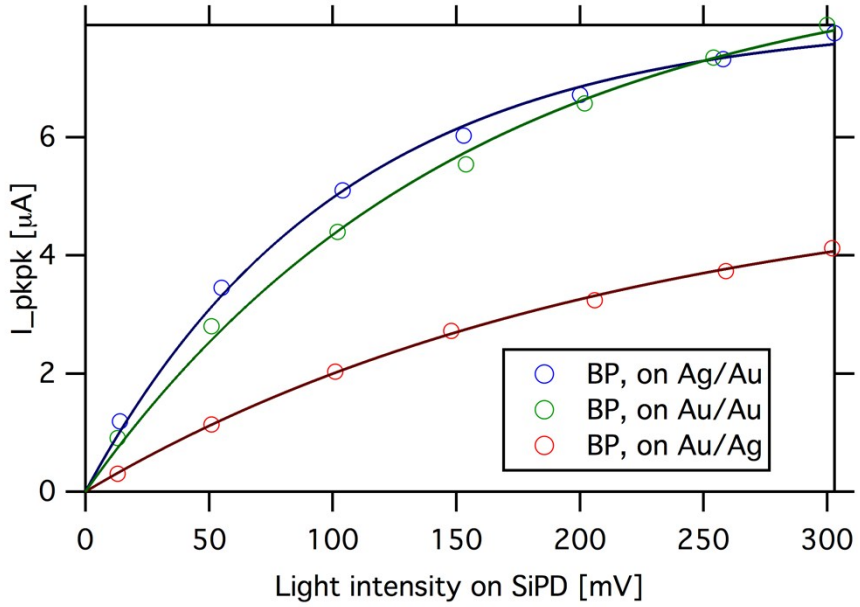

FIGURE S3c: Example of devices with sublinear dependence of $\boldsymbol{I_{peak}}$ *on light intensity when using a Au counter electrode. The ionic liquid used in these devices is BMIM* PF_6.

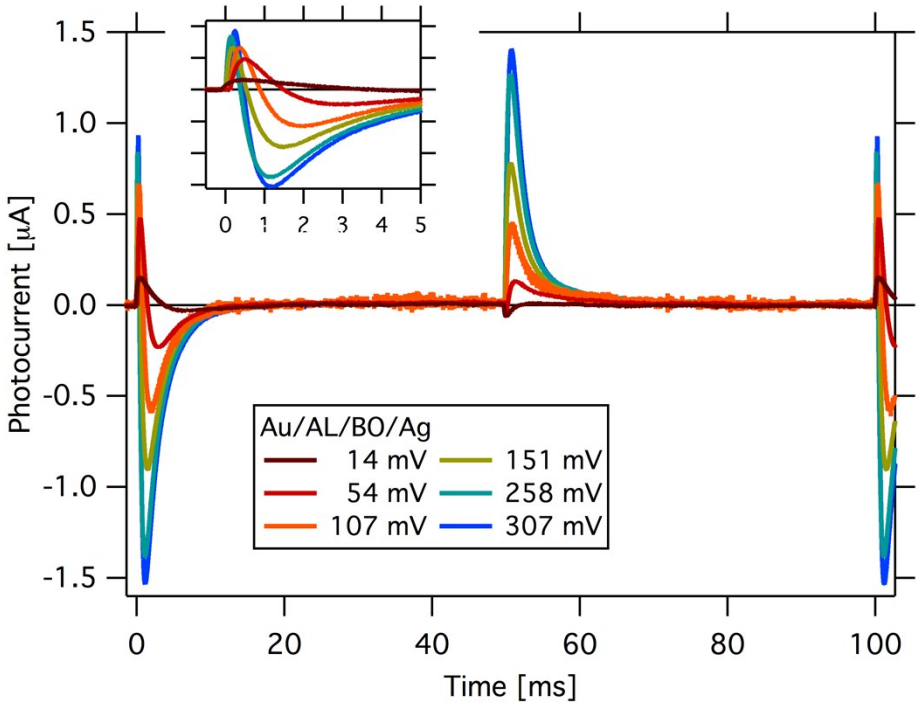

FIGURE S3d: Light intensity dependence of a signal showing hole extraction with consecutive electron extraction.

S4: Wavelength-dependence of photocurrent signal:

The non-linearity in signal shape (see section S3) can affect the acquisition of an action spectrum. In such a case, the use of a lock-in amplifier to measure the action spectrum is non-trivial, because the signal response depends on the shape of the input signal, and the change in shape for a light source with varying light power cannot be neglected. Furthermore, the light intensity has to be strong enough to ensure total penetration of the active layer, and thus homogeneous exciton generation. For the devices used in this study (minimum transmission = 60%), the light power used (see Fig. S4b) was sufficiently strong across the entire wavelength range to penetrate the whole film, as a difference in the action spectrum, depending on the reflectivity of the underlying metal, could be observed (Fig. S4a). The shape of the action spectrum was found to be independent of the ionic liquid used, and of the counter electrode material, if non-linearity could be avoided or corrected for. As expected, consistent with previous studies,[6] the charge-transfer band around 600 nm is enhanced, compared to the absorption profile.

a)

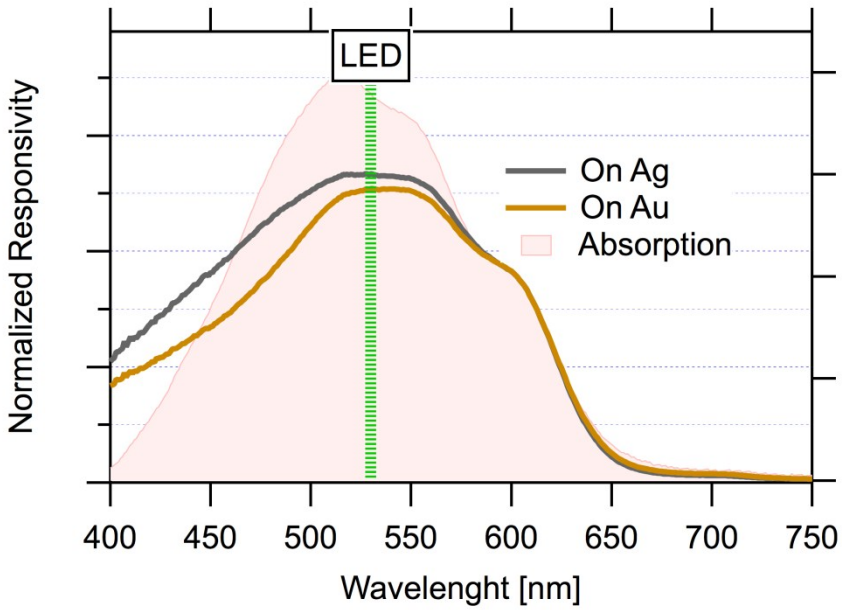

FIGURE S4a: Wavelength dependence of the responsivity of a 1:1 device depending on the active electrode material. The red shaded area corresponds to the absorption spectrum of a 1:1 P3HT:PCBM blend, corrected for scattering.

Methods: The wavelength-dependent transient photocurrent measurements were performed using a tungsten/halogen light source (Spectral Products ASBN-W 100 L) transmitted through a monochromator (Digikröm CM110, with a 1.2 mm grating) covering the 400−800 nm range (resolution 8-10 nm), with the light power not exceeding 150 μWcm^{-2}. The monochromated light power density was determined using a calibrated Si photodiode (see Fig. S4b). The incident light was mechanically

chopped (NF electronic instruments 5584A) at 83 Hz, unless otherwise stated. The light was focused through a pin-hole (2 mm) onto the active electrode (see Fig. S4c). The device was connected to a transimpedance amplifier (Femto, DLPCA200), which was connected to a lock-in amplifier (NF 5610B/A) and an oscilloscope (Tektronix, TBS1052B). The wavelength dependence was recorded using a home-written lab-view program, which allows multiple scans in forward and reverse direction at a minimal wavelength step of 0.1 nm. In order to ensure signal stabilization on the lock-in amplifier, a time step of at least 2 s was used. The responsivity was calculated from the peak of the photocurrent response on the oscilloscope.

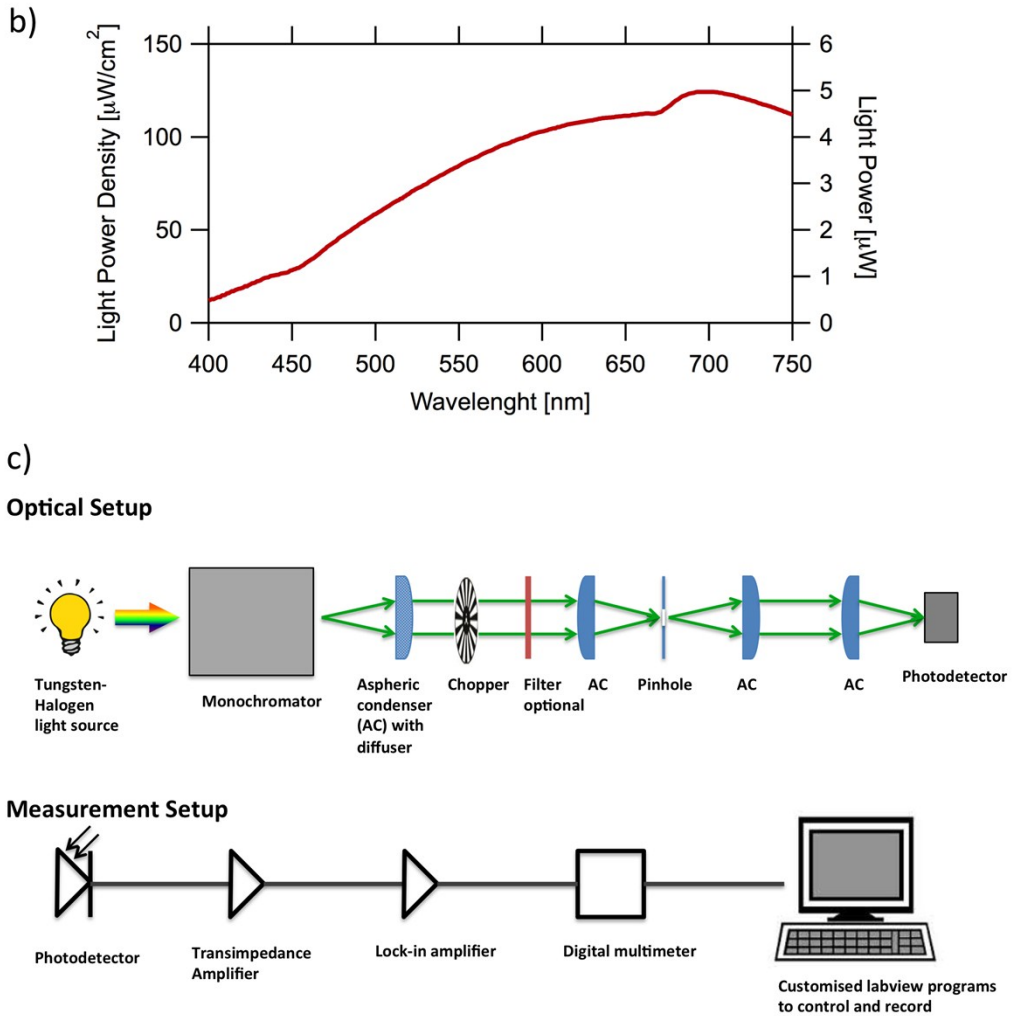

FIGURE S4b,c: Monochromated light intensity (b) and setup used for wavelength dependent measurements (c).

S5: Data analysis and fitting of the transient waveform:

For device comparison, a range of parameters were extracted from the transient waveform. For assessing the intensity of the signal $I_{peak} = |I_{peak,ON}| + |I_{peak,OFF}|$, the peak-to-peak distance was directly extracted from the waveform. In order to quantitatively analyze the shape of the transient signal, the data was fitted to a model equation (Eq. 1), derived empirically, and the fitting parameters were extracted. In general, a single exponential rise and double exponential decay function was sufficient to model the data:

$$I(t) = A_1 * \exp(-(t-t_0)/\tau_1) + A_2 * \exp(-(t-t_0)/\tau_2) - (A_1 + A_2) * \exp(-(t-t_0)/\tau_3) + y_0$$

where the first two exponents show the two contributions to the signal decay and the third exponent represents the rise, A_x are the amplitudes and τ_x the individual lifetimes, and t_0 and y_0 are the offsets. In many devices, the rise and decay times of the light ON peak were faster compared to those of the light OFF peak, which could be explained by the lower resistance within the active layer under illumination. The secondary slow decay of the photocurrent transient is assumed to come from either the repositioning of "trapped" charges within the active layer, or from the imbalance of carrier mobilities. The magnitude of the slow decay component of the photocurrent signal was comparably low for well-balanced active layers (quasi-ambipolar). The total charge Q extracted from the active layer is calculated by simple integration, and is given by:

$$Q = A_1 * \tau_1 + A_2 * \tau_2 - (A_1 + A_2) * \tau_3$$

The calculated values compared well with the values obtained by numerical integration.

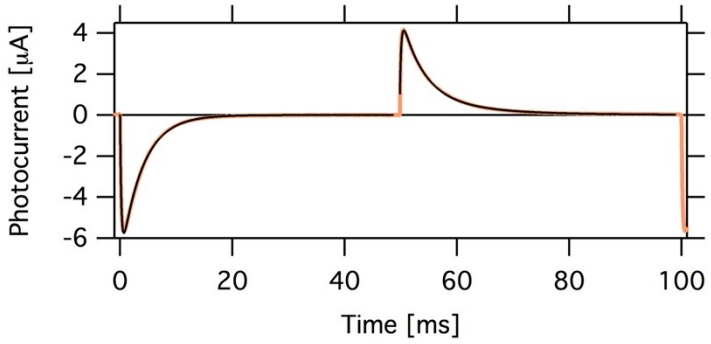

FIGURE S5: Fitting of the waveform of the initial response in Fig. 2(a) with a single rise single exponential decay for the light ON peak (A = -7.4 μA, tau1 = 3.8 ms, tau2 = 2.3 ms) and single rise double exponential decay for the light OFF peak (A1 = 4.0 μA, A2 = 1.2 μA, tau1a = 3.8 ms, tau1b = 10 ms, tau2 = 0.25 ms).

S6: Solid-state devices:

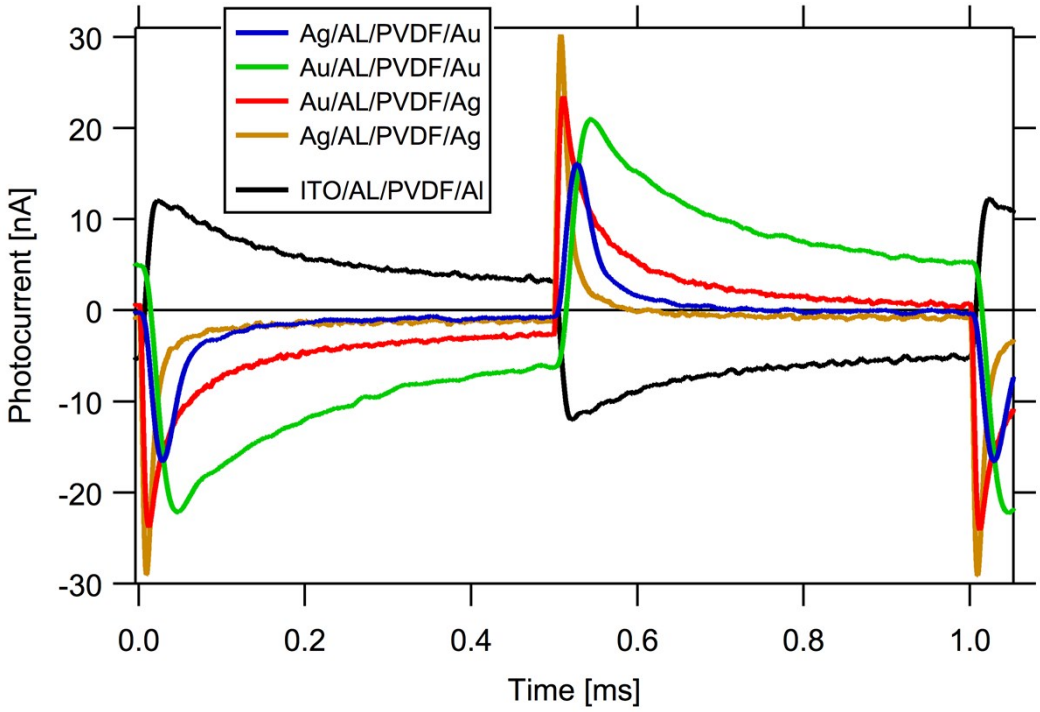

FIGURE S6: Photocurrent signal for solid-state devices depending on electrode configuration. The devices with an Au counter electrode were measured at 10^9 amplification, while the devices with an Ag counter electrode at 10^8 amplification. These devices were illuminated through the counter electrode (the photocurrent data was divided by the transmission to reduce to influence of the incident light intensity on the data). In the case of the ITO/Al device, the device was illuminated through the ITO. Also here, the PVDF layer was comparably thick, and the signal was measured at 10^8 amplification. It should be noted that the reproducibility in shape and intensity of the solid-state devices was greatly reduced by the variance of the PVDF layer, in terms of thickness and morphology,[7] and that the setup was not optimized for high speed/low responsivity devices (caused by the strongly reduced insulating layer capacitance), and thus it can be assumed that the signal shape is strongly affected by the measurement apparatus. However, none of these factors should have any effect on the observed signal polarity.

References

1. Tokuda, H.; Tsuzuki, S.; Susan, M.A.B.H.; Hayamizu, K.; Watanabe, M. *J. Phys. Chem. B,* **2006**, *110,* 19593-19600.

2. MSDS Data: a) N-(2-methoxyethyl)-N-methylpyrrolidinium bis(trifluoromethylsulfonyl)-imide; MSDS No. ION001-05064; Nisshinbo Holding: Japan, Aug. 27, 2014; b) N-Methyl-N-propylpiperidinium bis(trifluoromethanesulfonyl)imide; MSDS No. 26039; Kanto Chemical Co., Inc.: Japan, Mar. 8, 2010; c) 1-Butyl-3-methylimidazolium hexafluorophosphate; MSDS No. 05064; Kanto Chemical Co., Inc.: Japan, Apr. 26, 2004; d) 1-Ethyl-3-methylimidazolium tetrafluoroborate; MSDS No. 14644; Kanto Chemical Co., Inc.: Japan, Jun. 15, 2011; e) N-(2-methoxyethyl)-N-methylpyrrolidinium tetrafluoroborate; MSDS No. ION005-140801; Nisshinbo Holding: Japan, Aug. 27, 2014; f) 1-Ethyl-3-methylimidazolium ethylsulfate; MSDS No. 51682; Sigma Aldrich: UK, Jul. 31, 2012; g) 1-Allyl-3-butylimidazolium bromide; MSDS No. 01933; Kanto Chemical Co., Inc.: Japan, Jan. 20, 2010; h) Tributyldodecylphosphonium 2-trimethylsilylethanesulfonate; MSDS No. ION015-140801; Nisshinbo Holding: Japan, Aug. 7, 2014; i) Tributyldodecylphosphonium 2,2-dimethyl-2-silapentane-5-sulfonate; MSDS No. ION018-140801; Nisshinbo Holding: Japan, Aug. 7, 2014.

3. Fujimoto, T.; Matsushita, M.M.; Awaga, K. *J. Phys. Chem. C*, **2013**, *117*, 5552-5557.

4. Fukuoka, S. MSc Thesis, Nagoya University, Nagoya, Japan, Mar. 2014.

5. Reissig, L.; Dalgleish, S.; Awaga, K, *AIP Advances*, **2016**, *6*, 015306.

6. Li, B.; Dalgleish, S.; Miyoshi, Y.; Yoshikawa, H.; Matsushita, M. M.; Awaga, K. *Appl. Phys. Lett.* **2012**, *101*, 173302.

7. Dalgleish, S.; Matsushita, M. M.; Hu, L.; Li, B.; Yoshikawa, H.; Awaga, K. *J. Am. Chem. Soc.* **2012**, *134*, 12742-12750.